Four-step evolution of spin Hall conductance: Tight-binding electrons with Rashba coupling in a magnetic field

Yi-Fei Wang,[1,3] Yang Zhao,[1] and Chang-De Gong[1,2]
[1]*National Laboratory of Solid State Microstructures and Department of Physics, Nanjing University, Nanjing 210093, People's Republic of China*
[2]*Department of Physics, Suzhou University, Suzhou 215006, People's Republic of China*
[3]*Department of Physics, Zhejiang Normal University, Jinhua 321004, People's Republic of China*
(Received 23 January 2008; revised manuscript received 21 May 2008; published 2 July 2008; publisher error corrected 7 July 2008)

We report the investigation of magnetotransport properties of tight-binding electrons with Rashba spin-orbit coupling (SOC). Four-step evolutions of the spin Hall and charge-Hall conductances (SHC and CHC) have been found when fixing the magnetic field and tuning the Rashba SOC: the SHC shows size-dependent resonant jumps and even changes its sign; the CHC exhibits three successive quantum jumps. More arrestingly, such four-step evolutions are reflected in topological characters of edge states of a cylindrical system and are robust against weak disorder.

DOI: 10.1103/PhysRevB.78.045301 PACS number(s): 72.25.−b, 71.10.Ca, 71.70.Ej, 73.43.Cd

I. INTRODUCTION

Recently, the spin Hall effect (SHE), i.e., a generation of spin current perpendicular to an applied electric field,[1–4] has shed light on spintronics[5] and provided techniques to manipulate spins in nanostructures. In contrast to the extrinsic SHE driven by spin-orbit (SO) impurity scattering,[1] it is proposed that an intrinsic SHE exists in semiconductors with SO coupled bands.[2,3] These proposals encouraged the discovery of the SHE in GaAs semiconductor films and heterostructures[4] and in metallic Al films and Pt strips.[6] In models with SO coupled bands, two-dimensional electron gas (2DEG) with Rashba spin-orbit coupling (SOC) (Ref. 7) has the simplest form and is therefore most notable.[3,8–11] Meanwhile, tunable Rashba SOC has been achieved via an external gate voltage on the top of asymmetric heterostructures,[12] and the Rashba SO field in quantum wells and semiconductors can also be measured optically.[13]

In a clean 2DEG with parabolic dispersion and linear Rashba SOC, Sinova *et al.*[3] predicted that the spin Hall conductance (SHC) holds a universal value independent of SOC strength when both SO split bands are occupied. It is now known that such an intrinsic SHC with only linear Rashba SOC might be destroyed by any amount of disorder[10] or be canceled completely by intrabranch contributions in the presence of a magnetic flux.[8] In parallel, the SHC of 2DEG with linear Rashba SOC and Zeeman splitting in a magnetic field was calculated, and a resonant SHE was predicted when two Landau levels cross each other at the Fermi level.[11] In the presence of an underlying lattice potential, e.g., in metallic conductors such as Al films and Pt strips,[6] both parabolic dispersion and linear SOC should be modified and then incorporated into a lattice model which has been employed to study the effect of disorder on the SHE in the metallic regime.[9]

Here, we report the investigation of magnetotransport properties of tight-binding electrons (TBEs) with Rashba SOC. This model is also relevant to experimental systems such as ultracold fermions in an optical lattice with an effective SOC (Ref. 14) and graphene with an intrinsic or Rashba SOC.[15,16] Surprisingly, we have found that tuning the Rashba SOC strength generates four-step evolutions of the SHC and the charge-Hall conductance (CHC). Such bulk properties are also reflected in topological characters and spin polarizations of edge states of a cylindrical system and are robust against weak disorder.

II. FORMULATION

The model Hamiltonian of two-dimensional (2D) TBE on a square lattice with Rashba SOC and a uniform perpendicular magnetic field $\vec{B}=(0,0,-B)$ is[9]

$$H=-t\sum_{\langle ij\rangle}[e^{i\phi_{ij}}\hat{c}_i^{\dagger}\hat{c}_j+\text{H.c.}]+\lambda\sum_i[ie^{i\phi_{i,i+\vec{y}}}\hat{c}_i^{\dagger}\sigma_x\hat{c}_{i+\vec{y}}-ie^{i\phi_{i,i+\vec{x}}}\hat{c}_i^{\dagger}\sigma_y\hat{c}_{i+\vec{x}}+\text{H.c.}]-h_Z\sum_i(n_{i\uparrow}-n_{i\downarrow}),\qquad(1)$$

where $\hat{c}_i^{\dagger}=(c_{i\uparrow}^{\dagger},c_{i\downarrow}^{\dagger})$ are electron creation operators at site i, σ_x and σ_y are Pauli matrices, the nearest-neighbor hopping integral t will be taken as the unit of energy, λ is the Rashba SOC strength, and the Zeeman splitting parameter is $h_Z=\frac{1}{2}g\mu_B B$, with g as the Landé factor and μ_B as the Bohr magneton. We mainly consider $1/N$ magnetic-flux quantum per plaquette (N an integer), namely, $\phi=\Sigma_{\square}\phi_{ij}=2\pi Ba^2/\phi_0=2\pi/N$, with a as the lattice constant and $\phi_0=hc/e$ as the flux quantum. The Landau gauge $\vec{A}=(0,-Bx,0)$ and the corresponding periodical boundary conditions (PBCs) are adopted, and the magnetic unit cell has the size $N\times 1$.

After the numerical diagonalization of the Hamiltonian [Eq. (1)], the zero-temperature ($T=0$) CHC is calculated through the Kubo formula,[17]

$$\sigma_{\text{CH}}(E)=\frac{ie^2\hbar}{A}\sum_{\varepsilon_{m\mathbf{k}}<E}\sum_{\varepsilon_{n\mathbf{k}}>E}\times\frac{\langle m\mathbf{k}|v_x|n\mathbf{k}\rangle\langle n\mathbf{k}|v_y|m\mathbf{k}\rangle-\langle m\mathbf{k}|v_y|n\mathbf{k}\rangle\langle n\mathbf{k}|v_x|m\mathbf{k}\rangle}{(\varepsilon_{m\mathbf{k}}-\varepsilon_{n\mathbf{k}})^2},\qquad(2)$$

while the SHC at $T=0$ is given by[3]

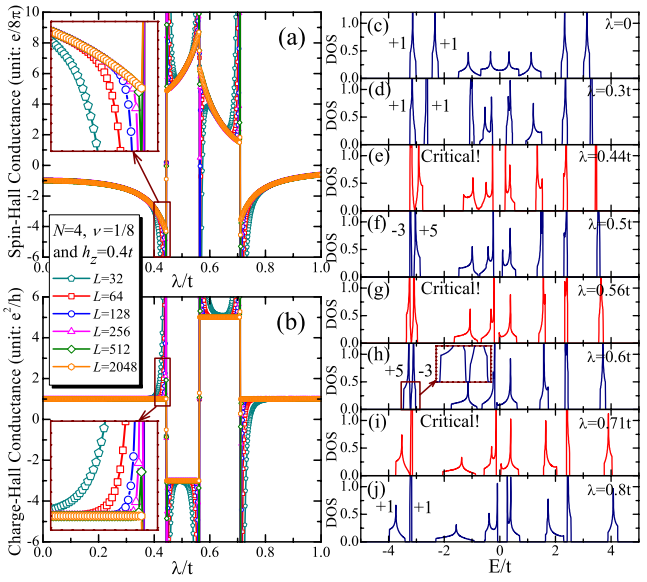

FIG. 1. (Color online) The case with $N=4$ and $h_Z=0.4t$. (a) The spin Hall conductance σ_{SH} versus the Rashba SOC parameter λ for electron filling $\nu=\frac{1}{8}$ and various lattice sizes. (b) The charge-Hall conductance σ_{CH} versus λ in the cases of (a). [(c)–(j)] The DOS for some λ's in (a). The Chern numbers of subbands are also shown.

$$\sigma_{\mathrm{SH}}(E) = -\frac{e\hbar}{A}\sum_{\varepsilon_{m\mathbf{k}}<E}\sum_{\varepsilon_{n\mathbf{k}}>E}\frac{\mathrm{Im}\langle m\mathbf{k}|J_x^{z\ \mathrm{spin}}|n\mathbf{k}\rangle\langle n\mathbf{k}|v_y|m\mathbf{k}\rangle}{(\varepsilon_{m\mathbf{k}}-\varepsilon_{n\mathbf{k}})^2}, \tag{3}$$

where $A=L\times L$ is the area of this 2D system, E is the Fermi energy, $\varepsilon_{m\mathbf{k}}$ is the corresponding eigenvalue of the eigenstate $|m\mathbf{k}\rangle$ of mth Landau subband, and the summation over wave vector $\mathbf{k}$ is restricted to the magnetic Brillouin zone (MBZ): $-\pi/N\le k_x a<\pi/N$ and $-\pi\le k_y a<\pi$. The velocity operator is defined as $\mathbf{v}=i/\hbar[H,\mathbf{R}]$ ($\mathbf{R}$ is the position operator of electron) and the spin current operator as $J_x^{z\ \mathrm{spin}}=\hbar/4\{v_x,\sigma_z\}$. When E falls in energy gaps, we can rewrite σ_{CH} as $\sigma_{\mathrm{CH}}(E)=e^2/h\Sigma_{\varepsilon_m<E}C_m$, where C_m is the Chern number[17] of the mth totally filled Landau subband.

III. EXAMPLE WITH $N=4$

An overall pictures of the CHC σ_{CH} and the SHC σ_{SH} calculated in Eqs. (2) and (3) are shown in Fig. 1 with $N=4$ (i.e., the flux strength $\phi=\frac{1}{4}\times 2\pi$), $h_Z=0.4t$, and various lattice sizes with $L=32-2048$. We concentrate on the lowest Landau subbands and consider the electron filling $\nu=\frac{1}{8}$.

In the case of $\lambda=0$ [Fig. 1(c)], the density of states (DOS) is symmetric about the Fermi energy E, and the lowest two Landau subbands (each totally filled subband contributes $\frac{1}{8}$ to ν) are well separated due to a sufficiently large Zeeman splitting ($h_Z=0.4t$); the lowest subband is occupied by spin-up electrons, while the second lowest one by spin-down electrons, and each subband carries a Chern number +1. With λ increasing from 0 to $1.0t$ one sees a systematic four-step evolution of σ_{CH} and σ_{SH} versus λ; there are three critical λ_c's at which both σ_{SH} and σ_{CH} exhibit jumps.

When λ increases from 0 to $\lambda_{c1}\approx 0.44t$, the lowest two Landau subbands approach each other, then merge together and form a pseudogap at λ_{c1} [Fig. 1(e)]; σ_{SH} changes continuously from $-1e/8\pi$ to larger negative values [Fig. 1(a)], while $\sigma_{\mathrm{CH}}=+1e^2/h$ nearly stays unchanged [Fig. 1(b)]. Here for a small lattice size ($L=32$), σ_{SH} and σ_{CH} both present divergence when λ approaches λ_{c1}. With the lattice size increased ($L=64-512$), the divergence is weakened accordingly; for $L=2048$, σ_{SH} approaches a finite value $-4.30e/8\pi$ at λ_{c1}, and σ_{CH} remains as $+1e^2/h$ for $0\le\lambda<\lambda_{c1}$. In the following, we focus on the data obtained with $L=2048$.

Increasing λ across each λ_c, σ_{SH} and σ_{CH} both exhibit sharp jumps: σ_{SH} jumps from -4.30 to $+4.87$ (in units of $e/8\pi$) at λ_{c1}, from $+8.71$ to $+6.32$ at $\lambda_{c2}\approx 0.56t$, and from $+1.49$ to -3.57 at $\lambda_{c3}\approx 0.71t$; σ_{CH} changes as $+1\to-3\to+5\to+1$ (in units of e^2/h). In intervals away from λ_c's, σ_{SH} varies continuously, while σ_{CH} remains unchanged. The corresponding DOS [Figs. 1(c)–1(j)] also points out that the lowest two Landau subbands approach, merge together and form a pseudogap at each λ_c, and then separate for three times.

Mainly, such a four-step evolution of the SHC of TBE is distinct from the resonant SHE of 2DEG predicted by Shen *et al.*[11] in four aspects: in 2DEG, two Landau levels cross each other at the Fermi level only once and produce one λ_c, while for TBE the two Landau subbands touch successively three times and result in three λ_c's; at a λ_c, the SHC of 2DEG diverges at $T=0$, while the SHC of TBE converges to finite values in the thermodynamic limit ($L\to\infty$) at $T=0$; the SHC of 2DEG does not change its sign, while the SHC of TBE changes its sign at λ_{c1} and λ_{c3}; furthermore, the CHC of 2DEG is unaffected when tuning λ, but the CHC of TBE presents three successive quantum jumps.

IV. CASES WITH WEAKER MAGNETIC FIELDS

The above four-step evolutions have also been verified by further numerical calculations of the cases with $N=4-16$, $h_Z=0.05t-0.4t$, and various ν's (with odd number of totally filled Landau subbands), as illustrated by four examples in Fig. 2. For $N=4$, $h_Z=0.2t$, and $\nu=1/8$ [Fig. 2(a)], σ_{SH} shows behaviors similar to that in Fig. 1(a) while with smaller λ_c's and narrower transition regions (i.e., smaller $\lambda_{c3}-\lambda_{c1}$); for $N=6$ and $N=8$ [Figs. 2(b)–2(d)], the transition regions are narrower than the case with $N=4$. Meanwhile, the quantized CHC also exhibits three jumps by $-Ne^2/h$, $+2Ne^2/h$, and $-Ne^2/h$.

In brief, the larger the N's, the significantly narrower the transition regions [$(\lambda_{c1}\le\lambda\le\lambda_{c3})$] are. However, the positive values in the transition regions are much larger, and the total weights of positive part of σ_{SH} (i.e., the integral from λ_{c1} to λ_{c3}) possessing the same order of magnitude are, respectively, 0.96, 1.69, 0.99, and 1.12 in the four cases of Fig. 2. [Note that the weight is 1.22 for the case in Fig. 1(a).] In the limit of large N, namely, when the lattice effect becomes negligible, the intermediate two steps of the four-step evolution will not be observable due to their negligible width of transition regions; three critical λ_c's are merged into only one; the resulting SHC exhibits a divergence at the only λ_c

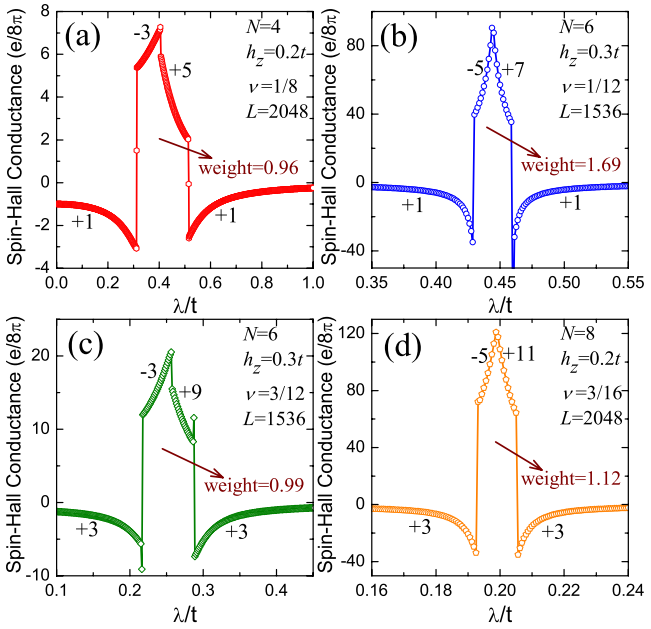

FIG. 2. (Color online) σ_{SH} versus the Rashba SOC parameter λ in various cases. σ_{CH} (in units of e^2/h) of each evolution step is also shown.

and is a reminiscence of the resonant SHE of 2DEG;[11] since the negligible width of transition region and the CHCs are the same at both sides of the only λ_c, such a behavior also coincides well with the resonant SHE of 2DEG in which tuning λ across a λ_c does not change the CHC.[11]

V. CASES WITH p/N FLUX QUANTUM PER PLAQUETTE

An interesting generalization is to consider the cases with $\phi=2\pi(p/N)$ (p and N are coprime integers), namely, p/N flux quantum per square plaquette (there are still $2N$ Landau subbands). For the cases with $p>1$ of TBE on a square lattice, based on a Diophantine equation,[17] a pattern of subband structure has been found by Yang and Bhatt:[18] the subbands away from the band center form groups with p subbands each, and the total Chern number of each group is +1 (although the Chern number within each group oscillates between positive and negative values depending sensitively on the specific values of p and N).

For the Rashba SOC $\lambda=0$ and given a sufficient large Zeeman splitting h_Z, the lowest several Landau subbands are all occupied with spin-up electrons and well separated from the higher Landau subbands of spin-down electrons. Now tuning λ from 0 to large values, we have also found four-step evolutions of the SHC in various cases with $p=3$ or 5, as shown in Fig. 3.

However, there are two kinds of four-step evolutions now. For the cases with electron filling $\nu=mp/(2N)$ and m is an integer [Figs. 3(b), 3(d), and 3(f)], every evolution step of SHC is very similar to the simple cases with $p=1$, except for a fine structure of a very narrow dip between the second and third evolution steps. Moreover for larger N, the additional dip structure becomes narrower and shallower. For the cases with electron filling $\nu=q/(2N)\neq mp/(2N)$ and q is also an

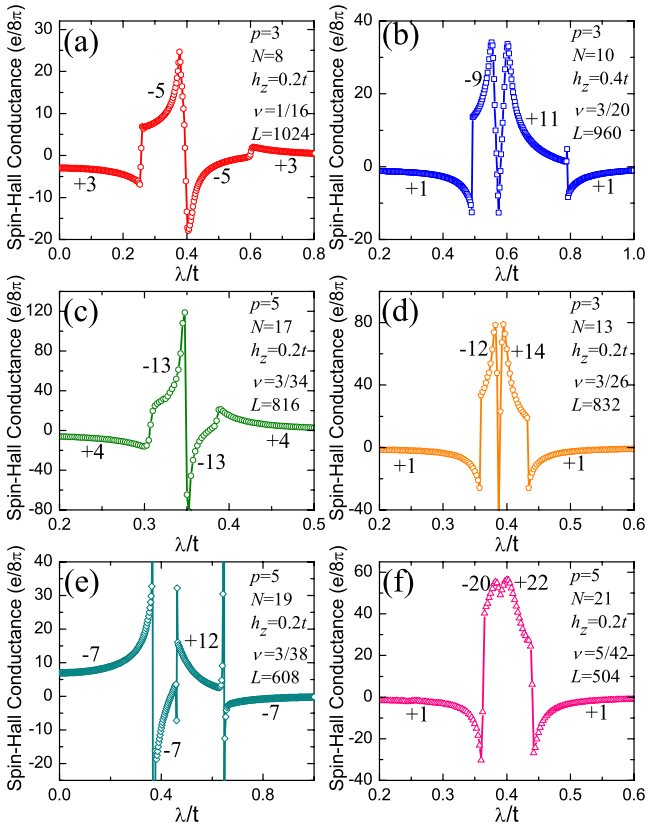

FIG. 3. (Color online) σ_{SH} versus λ for various cases with $\phi=2\pi(p/N)$: (a) $p=3$, $N=8$, and $\nu=1/16$; (b) $p=3$, $N=10$, and $\nu=3/20$; (c) $p=5$, $N=17$, and $\nu=3/34$; (d) $p=3$, $N=13$, and $\nu=3/26$; (e) $p=5$, $N=19$, and $\nu=3/38$; and (f) $p=5$, $N=21$, and $\nu=5/42$. σ_{CH} (in units of e^2/h) of each evolution step is also shown.

integer [Figs. 3(a), 3(c), and 3(e)], σ_{CH} and σ_{SH} of some evolution steps have opposite signs compared to the cases with $p=1$.

We should note the energy gaps of subbands within a group Δ^{intra}_{group}, which is much smaller than the energy gaps between two neighboring groups, Δ^{inter}_{group}. Taking the case of $p=3$ and $N=23$ (at $h_Z=0.1t$ and $\lambda=0$), $\Delta^{intra}_{group}\sim 0.002t$ for the first spin-up group (or the first spin-down group), $\Delta^{intra}_{group}\sim 0.01t$ for the second spin-up or spin-down group, and $\Delta^{intra}_{group}\sim 0.03t$ for the third spin-up or spin-down group, while $\Delta^{inter}_{group}\sim 1.3t$ between the first spin-up group and the second one, $\Delta^{inter}_{group}\sim 0.9t$ between the second spin-up group and the third one, and the energy gap Δ^{inter}_{group} between a Zeeman-splitted spin-up group and a spin-down one is of the order of $2h_Z=0.2t$. A weak disorder of the magnitude of Δ^{intra}_{group} will merge this group (consisting of p subbands and a total Chern number +1) which forms a big subband carrying a single Chern number +1.[18] As for the second kind of cases with $\nu=q/(2N)\neq mp/(2N)$, such a weak disorder will make the Fermi energy lie in this subband (hence render the system metallic), and there should be no four-step evolution anymore (since the four-step evolution requires the Fermi energy to lie in a well-defined energy gap when $\lambda=0$).

In contrast, since $\Delta^{inter}_{group}\gg\Delta^{intra}_{group}$, the first kind of cases with $\nu=mp/(2N)$, compared to the second one, requires less

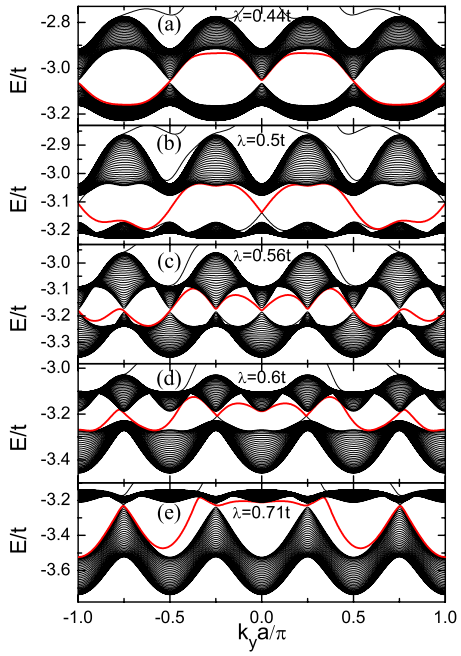

FIG. 4. (Color online) Lowest two subbands and intermediate edge states [shown as thick (red) lines] of a cylinder of the size $128\times\infty$ (OBC in the x direction and PBC in the y direction) with $N=4$, $h_Z=0.4$, and various λ's.

stringent experimental conditions. Moreover to observe the additional fine structure (namely, a narrow and shallow dip which is fragile to disorder), it also requires lower temperature and cleaner sample. Therefore, we believe that the four-step evolution is the major lattice effect, represents the major difference compared to 2DEG, and should be observed first under less stringent experimental conditions compared to the fine structures.

VI. EDGE STATES IN A CYLINDRICAL SYSTEM WITH $N=4$

An alternative way to reveal the distinctions among four evolution steps is to calculate the edge states of the system on a cylinder. These edge states reflect the topological character of the corresponding bulk state.[19,20] Just recently, spin-filtered edge states have been considered for a graphene cylinder with an intrinsic SOC (Ref. 15) (in a two-component Haldane model[21]) or Zeeman splitting,[22] a quantum SHE arising from helical edge states has been proposed and experimentally verified in HgTe quantum wells,[23] and edge states have also been employed to characterize topological band insulators and chiral spin liquids.[24] Now as an illustration, we take a cylinder of square lattice of the size $128\times\infty$ with $N=4$ (i.e., the flux strength $\phi=\frac{1}{4}\times 2\pi$) and apply open boundary condition (OBC) in the x direction and PBC in the y direction.

Chern numbers of bulk Landau subbands are intimately related to the winding numbers of the corresponding edge states.[20] For $\lambda_{c1}<\lambda<\lambda_{c2}$, there is one edge state winding three times from the upper subband to the lower one then back to the upper one [a thick (red) line in Fig. 4(b)] which corresponds to $C_1=-3$ (a Chern number of -3 of the lower subband). For $\lambda_{c2}<\lambda<\lambda_{c3}$, there is one edge state winding five times from the lower subband to the upper one then back to the lower one [Fig. 4(d)] which corresponds to $C_1=+5$. While for $0<\lambda<\lambda_{c1}$ or $\lambda_{c3}<\lambda<1.0t$ (not shown in Fig. 4), there is another edge state winding only once from the lower subband to the upper one then back to the lower one which corresponds to $C_1=+1$.

The continuum spectrum of this cylinder also gives further descriptions about the jumps of the bulk CHC. Increasing λ across λ_{c1} [Fig. 4(a)] or λ_{c3} [Fig. 4(e)], the lowest two subbands touch at four points simultaneously in k space and a Chern number of -4 is transferred from the upper subband to the lower one; while across λ_{c2} [Fig. 4(c)], the lowest two subbands touch at eight points simultaneously in k space and a Chern number of $+8$ is transferred between them. Such a correspondence between transferred Chern numbers and touching points in k space has also been verified for $N=5-8$. We remark that similar behaviors about the quantized jumps of the CHC have been discussed through a Diophantine equation of the next-nearest-neighbor TBE model[25] and numerical calculations of TBE modulated by a staggered magnetic flux.[26]

In addition, the spin polarization carried by the edge states can be computed explicitly as $P^z_{m\mathbf{k}}(i)=\hbar/2\langle m\mathbf{k}|\hat{c}_i^\dagger\sigma_z\hat{c}_i|m\mathbf{k}\rangle$, with i as the lattice site index in the x direction.[16] In Fig. 5, we plot the spin polarization P^z of some edge states of the above cylindrical system. If λ takes a value far away from λ_c's, P^z takes prominently large values near the left or the right edge and is almost zero in the intermediate region [Figs. 5(a), 5(c), and 5(f)–5(h)]; but if λ takes a value close to λ_c's, P^z fluctuates strongly between two edges [Figs. 5(b), 5(d), and 5(e)]. Note that for a fixed k_y, the dominantly positive peak of P^z moves to another edge when λ varies from $0.4t$ to $0.5t$. Moreover for edge states of $\lambda=0.8t$ [Fig. 5(h)], P^z takes prominently negative values near edges.

VII. PRESENCE OF DISORDER

We add a term $\Sigma_i w_i\hat{c}_i^\dagger\hat{c}_i$ (Ref. 9) into the Hamiltonian [Eq. (1)] to account for the effects of nonmagnetic disorder, with w_i being a random potential uniformly distributed between $[-W/2,W/2]$. For $N=4$, the adopted 100 random-potential configurations are of the size 8×8 (such a superunit cell is commensurate with the magnetic unit cell in the absence of disorder), and the total lattice is of the size 32×32. It can be seen from Fig. 6 that weak disorder ($W\leq 0.5t$) does not smear out the overall four-step evolution of the SHC. For stronger disorder ($W=2.0t$), the SHC does not show resonance anymore near λ_{c1} or λ_{c3} and takes positive values in an enlarged interval while the peak is diminished into a hump.

In order to check the effect of finite system size on the evolution of the SHC against disorder strength W, we adopt four series of random-potential configurations with, respectively, the sizes 4×4 (1000 configurations), 8×8 (100 configurations), 12×12 (20 configurations), and 16×16 (10 configurations). Moreover from the example with $\lambda=0.5t$ shown in the inset of Fig. 6, we can see that the evolutions of

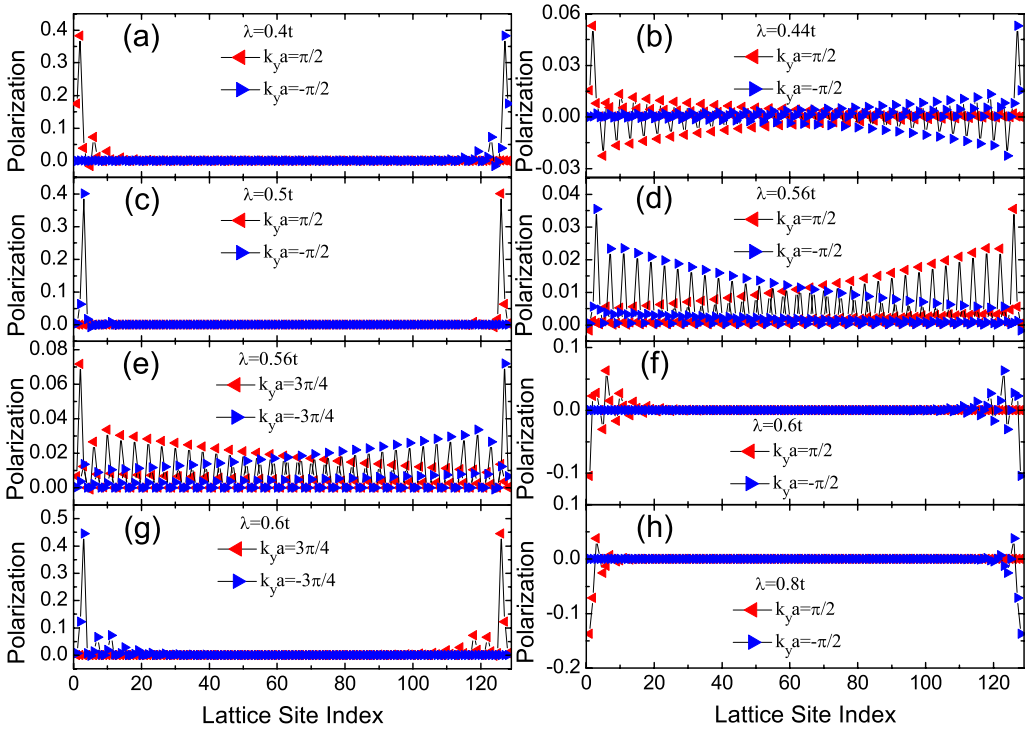

FIG. 5. (Color online) Spin polarization P^z (in units of $\hbar/2$) versus the lattice site index in the x direction for the edge states of the cylindrical system in Fig. 4.

σ_{SH} versus W coincide well for three larger sizes and hence are scarcely affected by the finite-size effect.

VIII. SUMMARY AND DISCUSSION

An intriguing evolution of magnetotransport property has been demonstrated by TBE with Rashba SOC in a magnetic field: (i) with the flux strength $\phi=2\pi/N$ and the Zeeman splitting fixed, when increasing the Rashba SOC λ from 0, four-step evolutions of the SHC and CHC have been observed; (ii) at three λ_c's, the SHC shows size-dependent resonances and jumps and changes its sign at λ_{c1} and λ_{c3}; (iii) meanwhile, the quantized CHC shows three successive jumps by $-Ne^2/h$, $+2Ne^2/h$, and $-Ne^2/h$; (iv) for smaller ϕ's, the total weights of positive part of SHC have the same order of magnitude although the transition regions are significantly narrower; (v) edge states of a cylindrical system reflect such bulk properties; (vi) this four-step evolution is robust against weak disorder; and (vii) for the flux strength $\phi=2\pi(p/N)$ ($p>1$ and N are coprime integers), there are possible fine structures in addition to the major four-step evolution.

As emphasized in the end of Sec. III, this four-step evolution of SHC is distinct from the resonant SHE of 2DEG.[11] To understand why such differences occur, we should note the following lattice effects: in the presence of a strong underlying lattice potential, a conventional Landau level (especially a higher Landau level) of 2DEG will acquire a finite width and expand into a Landau subband;[27,28] the Chern number of each Landau subband can take integer values other than +1 (Ref. 17) and change its value discretely[25,26] (by multiples of N) when two subbands cross each other and change their topological characters (e.g., winding numbers, Berry phases, or k-space curvatures). In contrast, a Landau level of 2DEG always has a Chern number of +1 if it is well separated from the others. One necessary experimental condition to observe such an evolution is similar to the requirement to observe the famous Hofstadter butterfly,[28] namely, the magnetic field should be strong enough or the lattice constant should be large enough (and the resulting N is not very large). To observe the step character unambiguously under an accessible uniform magnetic field with $N \gtrsim 100$, we

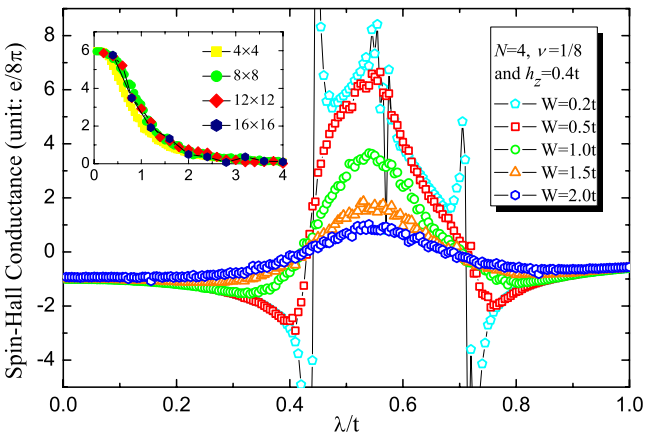

FIG. 6. (Color online) σ_{SH} versus λ in the case with $N=4$, $h_Z=0.4t$, and various disorder strength W's (100 random-potential configurations of the size 8×8). The inset shows the evolution of σ_{SH} versus W at $\lambda=0.5t$ for various sizes of random-potential configurations.

estimate that both the strength of disorder W and the temperature k_BT should not exceed $\frac{4t}{N} \sim \frac{4t}{100}$ (where $4t$ is half of the original bandwidth). Moreover since the phenomenon is attributed to the subband crossing induced the competition between the SOC and the Zeeman splitting, the SOC strength λ is required to be tunable and at the same energy scale of the Zeeman splitting energy h_Z. Moreover to observe the possible additional fine structure of the cases with the flux strength $\phi=2\pi(p/N)$ ($p>1$ and N are coprime integers), it requires much lower temperature and cleaner sample. Hence we believe the four-step evolution is the major lattice effect, represents the major difference compared to 2DEG, and should be observed first under less stringent experimental conditions compared to the fine structures.

Such an interesting four-step evolution of SHC is expected to occur in 2D electron systems with a strong lattice potential, a mechanism of SOC or SO scattering, and an external magnetic field. Some candidate experimental systems are metallic conductors such as Al films and Pt strips,[6] ultracold fermions in an optical lattice with an effective SOC,[14] and graphene with an intrinsic or Rashba SOC.[15,16] Moreover spin polarizations of edge states should be observable in a four-terminal experimental setup.[15,22]

ACKNOWLEDGMENTS

This work was supported by the National Nature Science Foundation of China (Grant No. 90503014), the State Key Program for Basic Researches of China (Grant No. 2006CB921802), the China Postdoctoral Science Foundation (Grant No. 20070410330), and the Jiangsu Planned Projects for Postdoctoral Research Funds (Grant No. 0602021C).

[1] M. I. D'yakonov and V. I. Perel', JETP Lett. **13**, 467 (1971); J. E. Hirsch, Phys. Rev. Lett. **83**, 1834 (1999); S. Zhang, *ibid.* **85**, 393 (2000).
[2] S. Murakami, N. Nagaosa, and S. C. Zhang, Science **301**, 1348 (2003).
[3] J. Sinova, D. Culcer, Q. Niu, N. A. Sinitsyn, T. Jungwirth, and A. H. MacDonald, Phys. Rev. Lett. **92**, 126603 (2004).
[4] Y. K. Kato, R. C. Myers, A. C. Gossard, and D. D. Awschalom, Science **306**, 1910 (2004); J. Wunderlich, B. Kaestner, J. Sinova, and T. Jungwirth, Phys. Rev. Lett. **94**, 047204 (2005).
[5] S. A. Wolf, D. D. Awschalom, R. A. Buhrman, J. M. Daughton, S. von Molnár, M. L. Roukes, A. Y. Chtchelkanova, and D. M. Treger, Science **294**, 1488 (2001); I. Žutić, J. Fabian, and S. Das Sarma, Rev. Mod. Phys. **76**, 323 (2004).
[6] S. O. Valenzuela and M. Tinkham, Nature (London) **442**, 176 (2006); T. Kimura, Y. Otani, T. Sato, S. Takahashi, and S. Maekawa, Phys. Rev. Lett. **98**, 156601 (2007).
[7] Y. A. Bychkov and E. I. Rashba, JETP Lett. **39**, 78 (1984); J. Phys. C **17**, 6039 (1984).
[8] E. I. Rashba, Phys. Rev. B, **70**, 201309(R) (2004).
[9] L. Sheng, D. N. Sheng, and C. S. Ting, Phys. Rev. Lett. **94**, 016602 (2005); D. N. Sheng, L. Sheng, Z. Y. Weng, and F. D. M. Haldane, Phys. Rev. B **72**, 153307 (2005).
[10] H. A. Engel, E. I. Rashba, and B. I. Halperin, in *Handbook of Magnetism and Advanced Magnetic Materials*, edited by H. Kronmüller and S. Parkin (Wiley, Chichester, UK, 2007), pp. 2858–2877.
[11] S. Q. Shen, M. Ma, X. C. Xie, and F. C. Zhang, Phys. Rev. Lett. **92**, 256603 (2004); F. C. Zhang and S. Q. Shen, Int. J. Mod. Phys. B **22**, 94 (2008).
[12] J. Nitta, T. Akazaki, H. Takayanagi, and T. Enoki, Phys. Rev. Lett. **78**, 1335 (1997).
[13] L. Meier, G. Salis, I. Shorubalko, E. Gini, S. Schön, and K. Ensslin, Nat. Phys. **3**, 650 (2007).
[14] T. D. Stanescu, C. Zhang, and V. Galitski, Phys. Rev. Lett. **99**, 110403 (2007).
[15] C. L. Kane and E. J. Mele, Phys. Rev. Lett. **95**, 146802 (2005); **95**, 226801 (2005).
[16] L. Sheng, D. N. Sheng, C. S. Ting, and F. D. M. Haldane, Phys. Rev. Lett. **95**, 136602 (2005); D. N. Sheng, Z. Y. Weng, L. Sheng, and F. D. M. Haldane, *ibid.* **97**, 036808 (2006).
[17] D. J. Thouless, M. Kohmoto, M. P. Nightingale, and M. den Nijs, Phys. Rev. Lett. **49**, 405 (1982).
[18] K. Yang and R. N. Bhatt, Phys. Rev. B **59**, 8144 (1999).
[19] B. I. Halperin, Phys. Rev. B **25**, 2185 (1982).
[20] Y. Hatsugai, Phys. Rev. Lett. **71**, 3697 (1993).
[21] F. D. M. Haldane, Phys. Rev. Lett. **61**, 2015 (1988).
[22] D. A. Abanin, P. A. Lee, and L. S. Levitov, Phys. Rev. Lett. **96**, 176803 (2006).
[23] B. A. Bernevig, T. L. Hughes, and S. C. Zhang, Science **314**, 1757 (2006); M. König, S. Wiedmann, C. Brüne, A. Roth, H. Buhmann, L. W. Molenkamp, X. L. Qi, and S. C. Zhang, *ibid.* **318**, 766 (2007).
[24] D. H. Lee, G. M. Zhang, and T. Xiang, Phys. Rev. Lett. **99**, 196805 (2007); H. Yao and S. A. Kivelson, *ibid.* **99**, 247203 (2007).
[25] Y. Hatsugai and M. Kohmoto, Phys. Rev. B **42**, 8282 (1990).
[26] Y. F. Wang and C. D. Gong, Phys. Rev. Lett. **98**, 096802 (2007).
[27] P. G. Harper, Proc. Phys. Soc., London, Sect. A **68**, 874 (1955).
[28] D. R. Hofstadter, Phys. Rev. B **14**, 2239 (1976).